Novel Local Shape-Adaptive Gyrification Index with Application to Brain Development

Ilwoo Lyu[1(✉)], Sun Hyung Kim[2], Jessica Bullins[2], John H. Gilmore[2], and Martin A. Styner[1,2]

[1] Department of Computer Science, University of North Carolina, Chapel Hill, NC, USA
{ilwoolyu,styner}@cs.unc.edu
[2] Department of Psychiatry, University of North Carolina, Chapel Hill, NC, USA

Abstract. Conventional approaches to quantification of the cortical folding employ a simple circular kernel. Such a kernel commonly covers multiple cortical gyral/sulcal regions that may be functionally unrelated and also often blurs local gyrification measurements. We propose a novel adaptive kernel for quantification of the local cortical folding, which incorporates neighboring gyral crowns and sulcal fundi. The proposed kernel is adaptively elongated to cover regions along the cortical folding patterns. The experimental results showed that the proposed kernel-based gyrification measure achieved a higher reproducibility in a multi-scan human phantom dataset and captured the cortical folding in a more shape-adaptive way than the conventional method. In early human brain development, we found positive correlations with age over most cortical regions as previously found as well as novel, refined regions of both positive and negative correlations undetectable by the conventional method.

Keywords: Adaptive kernel · Early brain development study · Hamilton-Jacobi PDE · Local gyrification index · Sulcal/gyral curves

1 Introduction

Cortical surface expansion in early brain development is a dynamic, complex process called cortical gyrification. However, quantification of the cortical gyrification is difficult due to the nature of the cortical shape, which is highly complex and variable across individuals. The cortical folding patterns are quite inconsistent depending on the cortical region, which further hampers an appropriate analysis of the gyrification process. Typically, there are two major components in quantification of the local gyrification: (1) a local metric and (2) a local region (size, shape, etc.) over which the gyrification is quantified by the local metric.

Several attempts have been made to various metrics of the cortical folding. The local gyrification index was measured in the 3D space via the area ratio between the outer hull and the pial surface [6,8]. An outer hull-free gyrification

M. Descoteaux et al. (Eds.): MICCAI 2017, Part I, LNCS 10433, pp. 31–39, 2017.
DOI: 10.1007/978-3-319-66182-7_4

index was also proposed in [4]. In [2], a local shape analysis was performed using the so-called shape complexity index to measure a local cortical shape change.

In contrast, there is yet a lack of methods that incorporate a kernel shape into the cortical folding. Currently, a popular way to quantify local gyrification in 3D employs a simple circular kernel over the cortical surface using Euclidean sphere [6,8] or geodesic distance [2]. Typically, such a kernel is employed without taking the cortical folding into account, and its size (e.g., $r = 20\,\text{mm}$ in [6]) easily covers multi-sulcal regions that could be functionally unrelated. Moreover, a simple circular shape is insufficient to capture local variability in a population such as widening/deepening within a single sulcus/gyrus. To the best of our knowledge, none of existing methods have proposed a cortical shape-adaptive kernel yet.

In this paper we propose a novel geodesic kernel along the cortical folding that is functionally related within a single sulcus/gyrus. The local gyrification index is then measured within the local region constrained by the proposed kernel. To achieve this, we classify two main categories of the cortical folding properties:

- At sulcal fundi/gyral crowns (valley/ridge focused region): elongated shape
- At sulcal banks (flat region): isotropic shape

Our main contributions are (1) local cortical shape-adaptive kernel and (2) early postnatal brain development revealed with more spatially refined results.

2 Wavefront Propagation

In this section, we briefly review wavefront propagation. Given a medium (tangent space) Ω and its boundary $\partial\Omega$ in $\mathbb{R}^2$, the minimum travel-time from one (or multiple) source $\in \partial\Omega$ to a point $\mathbf{x} \in \Omega$ in the medium, $u(\mathbf{x})$, holds the following propagation equation for some propagation speed function F:

$$\begin{aligned} \|\nabla u(\mathbf{x})\|\, F\left(\mathbf{x}, \frac{\nabla u(\mathbf{x})}{\|\nabla u(\mathbf{x})\|}\right) = 1, \qquad & \mathbf{x} \in \Omega \subset \mathbb{R}^2, \\ u(\mathbf{x}) = 0, \qquad & \mathbf{x} \in \partial\Omega. \end{aligned} \tag{1}$$

Such a formulation is the so-called Hamilton-Jacobi partial differential equation (H-J PDE). A special H-J PDE is called the eikonal equation with a constant speed. To determine wavefront propagation behavior, we consider a special 2×2 tensor $M(\mathbf{x})$ on the tangent plane such that

$$F\left(\mathbf{x}, \frac{\nabla u(\mathbf{x})}{\|\nabla u(\mathbf{x})\|}\right) = \frac{\nabla u(\mathbf{x})^T}{\|\nabla u(\mathbf{x})\|} M(\mathbf{x}) \frac{\nabla u(\mathbf{x})}{\|\nabla u(\mathbf{x})\|}. \tag{2}$$

M has an elliptic form along its eigenvectors if M is symmetric and positive. In this work, we use the ordered upwind method [7] akin to Dijkstra's algorithm.

3 Novel Local Shape-Adaptive Gyrification Index

Our objective is to design a cortical shape-adaptive kernel to capture the cortical folding for local gyrification index. In wavefront propagation, the desirable kernel can be redefined equivalently as follows:

- At sulcal fundi/gyral crowns: anisotropic speed faster along ridges/valleys
- At sulcal banks: isotropic speed at every direction

We focus on a tensor field design to follow the above properties. This can be achieved by two main steps: (1) local cortical region segmentation and (2) tensor estimation at every location of the surface. Figure 1 illustrates an overview of the proposed pipeline for the adaptive kernel-based gyrification measure.

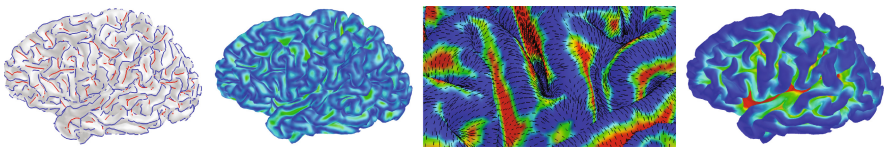

Fig. 1. An overview of the proposed pipeline. (a) Sulcal (*red*) and gyral (*blue*) curves are extracted for sulcal/gyral region segmentation. (b) The entire region segmentation is achieved via travel-time between the curves. (c) The travel-time map is normalized to capture sulci/gyri (*blue*) and sulcal banks (*red*); the gradients (*black*) of the travel-time map are obtained to create a tensor field. (d) The proposed local gyrification index map is obtained via the proposed kernel guided by the tensor field.

3.1 Outer Hull Creation and Surface Correspondence

Given a pial surface Ω, we create its outer hull H and establish a surface correspondence between them. A morphological closing operation is applied to Ω in the volume space to create H as proposed in [6]. We then apply the surface evolution method via solving the Laplacian equation modeled in [3] to guarantee a differentiable, bijective surface correspondence function $f : \mathbb{R}^3 \rightarrow \mathbb{R}^3$.

3.2 Travel-Time Map for Local Cortical Region Segmentation

We segment Ω to define a tensor at any location. We first find sulcal/gyral regions via the automatic curve extraction method [5], which follows the same idea [4] (see Fig. 1(a)). We then compute a travel-time map T from a set of the sulcal/gyral curves ζ to all locations of Ω. This is a standard shortest geodesic path problem at each point of Ω, which can be formulated by the eikonal Eq. (1), where $M = I$. We collect a set of points $\in \zeta$ to assign sources of the wavefront

propagation. With a boundary condition $T(\mathbf{p}) = 0$ for $\forall \mathbf{p} \in \zeta$, the H-J PDE (1) is simplified to

$$\|\nabla T(\mathbf{x})\| = 1. \tag{3}$$

The solution provides a travel-time map T of Ω as illustrated in Fig. 1(b).

3.3 Tensor Field

We compute a tensor field over Ω from T to guide an adaptive kernel. We aim at designing a kernel in which the propagation speed is getting anisotropic as it reaches sulcal/gyral regions. The tensor field is decomposed into two components: principal propagation directions and their associated propagation speeds.

Principal Propagation Direction. It is important to determine the propagation directions. The basic idea is to use the orthogonal and tangent directions to the sulcal/gyral curves. However, since the curves exist only in few cortical regions, we need something acting like the curves in other regions. To do so, we use the iso-travel-time contours of T. This is equivalent to finding shortest trajectories (orthogonal to the contours) of T between sulcal/gyral regions along the gradient field ∇T as studied in [7]. For $\forall \mathbf{x} \in \Omega$, its two principal propagation directions $\mathbf{v}_1(\mathbf{x})$ and $\mathbf{v}_2(\mathbf{x})$ are defined on the tangent plane:

$$\mathbf{v}_1(\mathbf{x}) = \frac{\nabla T(\mathbf{x})}{\|\nabla T(\mathbf{x})\|} \text{ and } \mathbf{v}_2(\mathbf{x}) = \frac{\nabla T^{\perp}(\mathbf{x})}{\|\nabla T^{\perp}(\mathbf{x})\|}, \tag{4}$$

such that $\nabla T(\mathbf{x}) \perp \nabla T^{\perp}(\mathbf{x})$. Consequently, $\mathbf{v}_1$ and $\mathbf{v}_2$ encode the tangent direction and the orthogonal direction to the geodesic trajectory between the corresponding sulcal fundus and gyral crown, respectively.

Principal Propagation Speed. The second modeling issue is to determine the speed associated with the principal propagation direction. It is desirable at sulcal fundi/gyral crowns that the speed has minimum and maximum along $\mathbf{v}_1$ and $\mathbf{v}_2$ whereas the speed needs to be almost the same along every direction at sulcal banks. At the middle of sulcal banks, however, their travel-time T is not identical as it varies at the depth of the corresponding sulcus. To address such an issue, we need a novel normalization with respect to local locations such that any location of Ω has a normalized travel-time ranging from η to 1 ($0 < \eta \leq 1$).

Given a point $\mathbf{x} \in \Omega$, we find the maximum travel-time among the shortest trajectories through $\mathbf{x}$ and then normalize the travel-time at $\mathbf{x}$ by the local maximum. We first find the source $\mathbf{s}_\mathbf{x} \in \zeta$ of $\mathbf{x}$ by tracing gradients over $-\nabla T$ until $T = 0$ while holding $T > 0$ and $T(\mathbf{x}) > T(\mathbf{x} - \nabla T d\mathbf{x})$. This gives a label map of Ω that represents the source of any point $\in \Omega$. Let $D_L(\mathbf{s})$ denote a region of Ω labeled by the same source $\mathbf{s} \in \zeta$, i.e., $D_L(\mathbf{s}) = \{\mathbf{x} \in \Omega | \mathbf{s}_\mathbf{x} = \mathbf{s}\}$. Similarly, the maximum travel-time through $\mathbf{x}$ is obtained by tracing over $\nabla T(D_L(\mathbf{s}_\mathbf{x}))$ until it touches a boundary of $D_L(\mathbf{s}_\mathbf{x})$. The normalized map S is then given by

$$S(\mathbf{x}) = (1 - \eta) \cdot \frac{T(\mathbf{x})}{T_{\max}(\mathbf{x})} + \eta, \tag{5}$$

where

$$T_{\max}(\mathbf{x}) = \max_{\mathbf{y} \in D_L(\mathbf{s}_\mathbf{x})} T(\mathbf{y}). \tag{6}$$

Thus, S captures region types in an easy way; for example, $S(\mathbf{x}) = 1$ (the middle of a sulcal bank) as shown in Fig. 1(c). We can consistently assign S and S^{-1} to the speed along $\mathbf{v}_1$ and $\mathbf{v}_2$, respectively. This guarantees the amount of the propagation at any point is constant, which is equal to 1.

Tensor Matrix. From (4) and (5), the tensor matrix $\tilde{M}$ is defined as follows:

$$\tilde{M}(\mathbf{x}) = S(\mathbf{x}) \cdot \mathbf{v}_1(\mathbf{x})\mathbf{v}_1(\mathbf{x})^T + S(\mathbf{x})^{-1} \cdot \mathbf{v}_2(\mathbf{x})\mathbf{v}_2(\mathbf{x})^T. \tag{7}$$

$\tilde{M}(\mathbf{x})$ guides the spatial-varying wavefront propagation. We recall η is used to prevent $\tilde{M}$ from being degenerative. The minimum bound η is thus employed as a regularization term. The speed tensor $\tilde{M}$ becomes isotropic when $\eta = 1.0$. Figure 2 shows behaviors of the proposed kernel varying in η.

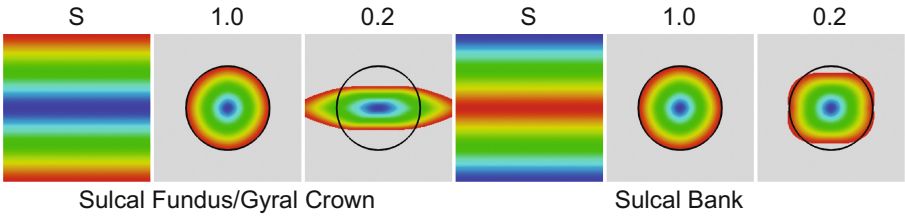

Fig. 2. Two simulated types and their kernel shapes by varying η. The respective travel-time maps S are obtained from the middle and marginal horizontal (*blue*) sources (1st and 4th columns). The kernel at sulcal fundus/gyral crown is elongated as η becomes small whereas it remains isotropic at sulcal bank even with a small value of η.

3.4 Adaptive Kernel and Local Gyrification Index

The proposed kernel at $\mathbf{x} \in \Omega$ is straightforwardly obtained by solving the H-J PDE equipped with $\tilde{M}$. In contrast to conventional methods, we use the cortical surface to define the kernel shape specifically suitable to the cortical folding while the kernel size is determined on the outer hull. Formally, the wavefront propagation guided by $\tilde{M}$ is formulated via the H-J PDE that satisfies the following equation with a boundary condition $K(\mathbf{x}) = 0$.

$$\|\nabla K(\mathbf{x})\| \cdot \left(\frac{\nabla K(\mathbf{x})^T}{\|\nabla K(\mathbf{x})\|} \tilde{M}(\mathbf{x}) \frac{\nabla K(\mathbf{x})}{\|\nabla K(\mathbf{x})\|} \right) = 1. \tag{8}$$

We then create a kernel by tracing one of the iso-travel-time contours of K. To select a proper iso-travel-time contour at $\mathbf{x}$ for the adaptive kernel creation, we

project all the iso-travel-time contours of K onto H via f. Then, we pick a projected iso-travel-time contour such that the area contained by the contour over H is equal to some positive constant (user-defined parameter). We assume that Ω is parametrized by $\varphi : \mathbb{R}^2 \to \mathbb{R}^3$ such that $\varphi(u, v) = (x(u, v), y(u, v), z(u, v)) \in \Omega$. Given K and travel-time $\delta \in \mathbb{R}^+$, we formulate the corresponding area of H to the iso-travel-time contour $(T = \delta)$ as the following surface integral.

$$A_H(\mathbf{x}; \delta) = \iint_{D_A(\mathbf{x};\delta)} \left\| \frac{\partial(f \circ \varphi)}{\partial u} \times \frac{\partial(f \circ \varphi)}{\partial v} \right\| dudv, \tag{9}$$

where $D_A(\mathbf{x}; \delta) = \{(u, v) \in \mathbb{R}^2 | K(\varphi(u, v)) \leq \delta\}$. Our resulting kernel is then determined by fixing the corresponding area of H by finding δ such that $A_H(\mathbf{x}; \delta)$ is equal to some constant function $\rho(\delta) \in \mathbb{R}^+$. Once δ is obtained by solving (9), we can compute the surface area of Ω governed by δ as follows.

$$A_\Omega(\mathbf{x}; \delta) = \iint_{D_A(\mathbf{x};\delta)} \left\| \frac{\partial \varphi}{\partial u} \times \frac{\partial \varphi}{\partial v} \right\| dudv. \tag{10}$$

From (9) and (10), the proposed gyrification index is given by the area ratio

$$lGI(\mathbf{x}; \rho(\delta)) = \frac{A_\Omega(\mathbf{x}; \delta)}{A_H(\mathbf{x}; \delta)} = \frac{1}{\rho(\delta)} A_\Omega(\mathbf{x}; \delta). \tag{11}$$

Figure 3 shows different kernels applied to the human cortex with $\rho = 316\,\mathrm{mm}^2$.

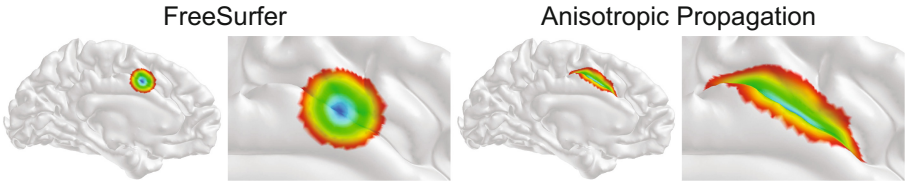

Fig. 3. Kernels at an arbitrary sulcal point on the same subject using different approaches with a fixed area on the outer hull $\rho = 316\ mm^2$. The circular kernel (intersection of the outer hull and the sphere) is obtained in FreeSurfer (*left*). The proposed kernel is obtained with $\eta = 0.5$ (*right*). The color indicates iso-travel-time contours.

4 Reproducibility

We evaluated the reproducibility of the proposed local gyrification index using a large set of scan/rescan data. A human phantom (male, age 26 at the start of this study) was scanned at the four different imaging sites, equipped with a Siemens 3T Tim Trio scanner at irregular intervals over the period of 2.5 years.

The same scanning sequences were employed for the developmental MRI scans, and 36 scans were acquired in total. Only the left hemispheres were reconstructed with 163,842 vertices via the FreeSurfer pipeline.

We computed the local gyrification index using the conventional method [6] and the proposed kernel. We varied the kernel area on the outer hull $\rho = 316$ and 1,264 mm^2 with an interval of 316 mm^2 for $\eta = 1.0$, 0.5, and 0.2. Specifically, 316 mm^2 is the minimum kernel size that fully spans any sulcal region (i.e., at least two gyral crowns), and 1,264 mm^2 is a typical kernel size used in [6]. Since the gyrification index is unitless, we used a coefficient of variation that quantifies how local gyrification indices vary across multiple scans. Table 1 summarizes the average reproducibility over the entire surface for both methods. As expected, a slightly lower reproducibility is achieved in the anisotropic propagation than in the isotropic propagation due to a less influence of sulcal/gyral patterns that might further introduce curve extraction errors in measurement. Even if so, however, the proposed method still achieves a better reproducibility than [6] at least in this multi-scan human phantom dataset.

Table 1. Coefficient of variation of gyrification index in multi-scan dataset (unit: %)

Area (mm^2)	316	632	948	1,264
Radius (mm)	10	14	17	20
FreeSurfer [6]	7.17 ± 7.84	4.87 ± 2.12	3.93 ± 1.65	3.11 ± 1.29
$\eta = 1.0$	3.64 ± 1.57	2.67 ± 1.05	2.31 ± 0.89	2.13 ± 0.79
$\eta = 0.5$	4.16 ± 1.49	3.18 ± 1.04	2.76 ± 0.88	2.52 ± 0.80
$\eta = 0.2$	4.78 ± 1.60	3.74 ± 1.17	3.26 ± 1.00	2.96 ± 0.92

5 Longitudinal Study in Early Postnatal Phase

As a part of early brain development studies (EBDS) [1], infant subjects were scanned shortly after birth, at age 1 year, and at age 2 years with both Siemens Allegra and Siemens Timm Trio head-only 3 T scanners. Both hemispheres were reconstructed with 163,842 vertices via the FreeSurfer pipeline. Table 2 summarizes a population statistics of the EBDS dataset used in this experiment.

We designed a linear mixed-effects model to investigate brain development in the early postnatal phase. The local gyrification index was used as a dependent variable Y with several fixed effects: postnatal age at scan, sex, and gestational age at birth. For each subject i, the following linear mixed-effects model was fitted with an interaction between the fixed effects and the subject-specific random effects U_i. We used SurfStat [9] for this analysis.

$$Y_i = \beta_0 + \beta_{\texttt{Age}}\texttt{Age}_i + \beta_{\texttt{Sex}}\texttt{Sex}_i + \beta_{\texttt{Gest}}\texttt{Gest}_i + U_i + \varepsilon_i, \tag{12}$$

where ε_i is an error term. The standard false discovery rate (FDR) correction was applied to correct multiple comparisons. Since the cortical surface area dramatically changes over ages, we further regularized the kernel size that corresponds to that of $r = 8$ (16) mm used in [6]: 108 (432), 180 (720), and 200 (800) mm^2 at neonate, 1 year, and 2 years, respectively. At age 2, the minimum size is 200 mm^2 that fully spans any sulcal region, and a typical size suggested in [6] is 800 mm^2. To handle the inter-subject variability in cortical surface area, we adaptively rescaled the kernel size for each subject according to the corresponding age group. Due to a trade-off between the reproducibility and measure accuracy, we set $\eta = 0.2$ to adaptively capture the cortical folding while keeping a comparable reproducibility to [6]. The same adjusted kernel size was employed for fair comparisons of age effect. Figure 4 shows that the proposed method yields spatially refined results as the proposed kernel adaptively captures local gyrification along the cortical folding while the overall patterns remain largely similar to [6]. Such refined patterns are likely due to different growth rates across cortex such as the myelination process. It is noteworthy that we aim not at capturing better statistical significance but at showing more refined resolution of t-maps.

Table 2. Early brain development studies (EBDS) dataset with population statistics

Scans	Total number	Male	Female	Age (days)	Age range	Gestational age (days)
Neonate	178	88	90	20.89 ± 9.50	6–68	275.27 ± 11.29
1 year	85	44	41	385.27 ± 22.84	343–481	273.36 ± 11.86
2 years	76	44	32	746.54 ± 25.03	693–827	272.62 ± 14.04
Total	339	176	163	-	-	274.20 ± 12.12

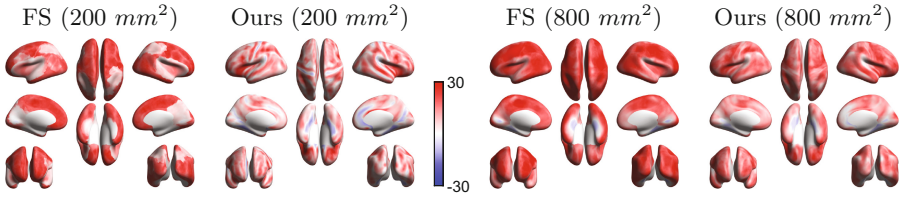

Fig. 4. Multi-comparison corrected t-maps for the local gyrification index change from neonate to 2-year-old using adjusted kernel sizes. FreeSurfer captures overall blurred measurements across the entire cortex whereas the proposed method reveals correlations with a high resolution of the measurements along the cortical folding.

6 Conclusion

We presented a novel cortical shape-adaptive kernel for local gyrification index. In contrast to a typical geodesic kernel, the proposed kernel is adaptively

elongated along the cortical folding via the well-defined H-J PDE. In the experiment, the significant regions were spatially refined along the cortical folding while the overall patterns were similar to the conventional method. Although the proposed method achieved a high reproducibility even with fast anisotropic speed, its performance could depend on a quality of the sulcal/gyral curve extraction. In the future, we will further validate our method regarding the preprocessing.

References

1. Gilmore, J.H., Shi, F., Woolson, S.L., Knickmeyer, R.C., Short, S.J., Lin, W., Zhu, H., Hamer, R.M., et al.: Longitudinal development of cortical and subcortical gray matter from birth to 2 years. Cereb. Cortex **22**(11), 2478–2485 (2012)
2. Kim, S.H., Lyu, I., Fonov, V.S., Vachet, C., Hazlett, H.C., Smith, R.G., Piven, J., et al.: Development of cortical shape in the human brain from 6 to 24months of age via a novel measure of shape complexity. NeuroImage **135**, 163–176 (2016)
3. Lee, J., Kim, S.H., Oguz, I., Styner, M.A.: Enhanced cortical thickness measurements for rodent brains via lagrangian-based RK4 streamline computation. In: Medical Imaging, p. 97840B. SPIE (2016)
4. Lyu, I., Kim, S.H., Styner, M.A.: Cortical surface shape assessment via sulcal/gyral curve-based gyrification index. In: 2016 IEEE 13th ISBI, pp. 221–224. IEEE (2016)
5. Lyu, I., Kim, S.H., Styner, M.A.: Automatic sulcal curve extraction on the human cortical surface. In: Medical Imaging, vol. 9413, p. 941324-1-7. SPIE (2015)
6. Schaer, M., Cuadra, M.B., Tamarit, L., Lazeyras, F., Eliez, S., Thiran, J.P.: A surface-based approach to quantify local cortical gyrification. IEEE Trans. Med. Imaging **27**(2), 161–170 (2008)
7. Sethian, J.A., Vladimirsky, A.: Ordered upwind methods for static Hamilton-Jacobi equations. SIAM J. Numer. Anal. **41**(1), 325–363 (2003)
8. Toro, R., Perron, M., Pike, B., Richer, L., Veillette, S., et al.: Brain size and folding of the human cerebral cortex. Cereb. Cortex **18**(10), 2352–2357 (2008)
9. Worsley, K., Taylor, J.E., Carbonell, F., et al.: SurfStat: a matlab toolbox for the statistical analysis of univariate and multivariate surface and volumetric data using linear mixed effects models and random field theory. Neuroimage **47**, S102 (2009)